Computers and Concrete, Vol. 10, No. 2 (2012) 105-119
DOI: http://dx.doi.org/10.12989/cac.2012.10.2.105

Flexural performance and fiber distribution of an extruded DFRCC panel

Bang Yeon Lee[1], Byung-Chan Han[2], Chang-Geun Cho[3] and Yun Yong Kim*[4]

[1]School of Architecture, Chonnam National University, Gwangju, Korea
[2]Department of Remolding Architecture, Woosong Information College, Daejeon 300-715, Korea
[3]School of Architecture, Chosun University, Gwangju, Korea
[4]Chungnam National University, Daejeon, Korea

(Received March 10, 2011, Revised November 2, 2011, Accepted November 9, 2011)

Abstract. This paper presents the mix composition and production method that was applied to an extruded Ductile Fiber Reinforced Cement Composite (DFRCC) panel, as well as the flexural performance, represented by deformation hardening behavior with multiple cracking. The effect of fiber distribution characteristics on the flexural behavior of the panel is also addressed. In order to demonstrate the fiber distribution effect, a series of experiments and analyses, including a sectional image analysis and micro-mechanical analysis, was performed. From the experimental and analysis results, it was found that the flexural behavior of the panel was highly affected by a slight variation in the mix composition. In terms of the average fiber orientation, the fiber distribution was found to be similar to that derived under the assumption of a two-dimensional random distribution, irrespective of the mix composition. In contrast, the probability density function for the fiber orientation was measured to vary depending on the mix composition.

Keywords: extruded DFRCC panel; image analysis; fiber distribution; flexural behavior.

1. Introduction

An Ductile Fiber Reinforced Cement Composite (DFRCC) is a pseudo deformation hardening cementitious composite that exhibits high deformation capacity while bridging micro-cracks by fibers, which in turn, leads to multiple cracking (Leung 1996, Lee *et al.* 2010a, Li and Leung 1992, Marshall and Cox 1988, Roth *et al.* 2010). The production methods of DFRCC include casting in place and spray. In addition to these methods, an extrusion process can be adopted. An extruded DFRCC panel is a precast composite that is fabricated by extrusion molding of cement, silica, sepiolite, natural minerals and fibers to enhance flexural strength and stiffness. The application of extrusion molding to DFRCC enhances the strength, elastic modulus and ductility of DFRCC. This stems from the lower porosity of extruded composites due to mechanical compaction, as well as the aligned orientation of fibers. Since the fibers are aligned in the normal direction of the crack surface, which corresponds with that of extrusion, the fibers that are aligned in that direction enhance the crack resistance more than the fibers that are oriented in three- or two-dimensional random distributions. Shao and Shah (1997), Shao *et al.* (1995), Stang and Li (1999), Akkaya *et al.* (2000) and Takashima *et al.* (2003) performed fundamental research

* Corresponding author, Professor, E-mail: yunkim@cnu.ac.kr

for evaluating the mechanical properties of extruded DFRCC. Fu and Lauke (1996) investigated the effect of fiber length and fiber orientation distributions on the tensile strength of short-fiber-reinforced polymers. However, there have been few studies on mix proportion, fiber orientation and dispersion, and the quantitative effect of the fiber distribution on the flexural behavior of an extruded DFRCC panel.

Therefore, this paper presents the mix composition, production method and curing conditions that were applied to an extruded DFRCC panel and the effect of the fiber distribution characteristics on the flexural behavior of the panel. In order to evaluate the effect of the fiber distribution characteristics on the flexural behavior, an image processing technique was applied. Based on the results, the influence of the fiber distribution characteristics on the mechanical properties, represented here by flexural strength, of an extruded DFRCC was quantitatively evaluated. A micro-mechanical analysis was also performed to evaluate whether the specimens satisfied the conditions for pseudo deformation hardening behavior based on multiple cracking.

2. Extruded DFRCC panel

2.1 Theoretical condition for pseudo deformation hardening behavior

To achieve pseudo deformation hardening behavior based on multiple cracking, the strength condition and energy condition should be satisfied. The strength condition is expressed in Eq. (1)

$$\sigma_0 > \sigma_{fc} \tag{1}$$

where σ_0 is the maximum bridging stress and σ_{fc} is the first cracking strength of the matrix. If the strength condition is satisfied, an immediate stress drop being pulled out or ruptured is prevented after initial cracking with bridging fibers. The energy condition is for steady state cracking (Marshall and Cox 1988). For multiple cracking behavior, a crack should be propagated under constant stress and with a constant crack opening in order to achieve a uniform stress distribution of fibers. This condition can be defined by the energy balance between the external work, the fracture energy needed to propagate the matrix crack and the energy dissipated by the bridging fibers. Eq. (2) expresses the energy balance for steady state cracking.

$$\sigma_s \delta_s = J_{tip} + \int_0^{\delta_s} \sigma_s(\delta) d\delta \tag{2}$$

where σ_s and δ_s are the stress in steady state cracking and the corresponding crack opening. J_{tip} is the fracture energy required to propagate the matrix crack. Based on these two criteria, the theoretical condition for pseudo deformation hardening behavior on the basis of multiple cracking can be expressed, as given, in Eq. (3)

$$J_{tip} = \sigma_s \delta_s - \int_0^{\delta_s} \sigma_s(\delta) d\delta < \sigma_0 \delta_0 - \int_0^{\delta_o} \sigma(\delta) d\delta = J'_b \tag{3}$$

J'_b denotes the complementary energy in the bridging curve. In Eq. (3), J'_b should be large enough to ensure steady-state cracking in spite of initial imperfections or defects by unexpected loads. Kanda and Li (2006) suggested a practical energy criterion as expressed in Eq. (4). Micromechanical analysis results for the extruded DFRCC developed in this study are described in Section 4.3.

$$\frac{J'_b}{J_{tip}} > 3.0 \tag{4}$$

2.2 Extrusion of DFRCC

2.2.1 Material

The physical and chemical properties of materials used for manufacturing the extruded DFRCC panel are listed in Table 1. Ordinary Portland cement with a density of 3.15 g/cm^3 and DFRCC powder were used as binders. The DFRCC powder was composed of pulverulent materials that strengthened the matrix and enhanced fire resistance. Silica powder with a density of 2.66 g/cm^3 and a specific surface of 3.79 cm^2/g, as well as silica sand with a density of 2.64 g/cm^3 and an average diameter of 0.2 mm were used as gravel. PVA fibers with a diameter of 39 μm and a length of 6~8 mm were used. The physical and chemical characteristics of the fibers are also listed in Table 2.

Table 1 Physical/chemical properties of materials

Types	OPC	Silica powder	Silica sand
Density (g/cm^3)	3.15	2.66	2.64
Fineness (cm^2/g)	3630	3793	0.2*
SiO_2	22.73	95.5	96.9
Al_2O_3	5.93	1.95	1.44
Fe_2O_3	3.37	0.76	0.34
CaO	61.73	-	0.11
MgO	2.53	-	0.03
SO_3	1.97	-	-
Ig.loss	1.74	1.79	-

*Diameter (mm)

Table 2 Properties of fibers

Ingredient	Polyvinylalchol (PVA)
Density (g/mm^3)	1.3
Length (mm)	6~8
Diameter (μm)	39
Surface treatment	Oiling agent
Melting point (^{o}C)	170
Thermal decomposition (^{o}C)	263
Tensile strength (MPa)	1700
Young's modulus (GPa)	29.4
Elongation (%)	3~113
Alkali resistance	High

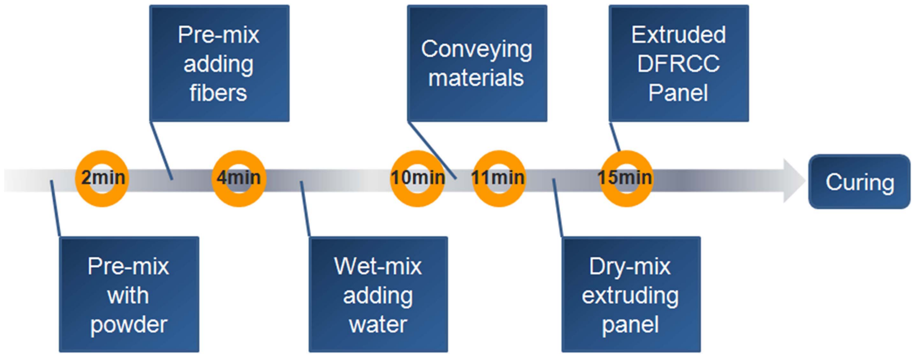

Fig. 1 Mixing sequence of extruded DFRCC panel

Fig. 2 Extrusion equipment

2.2.2 Production process

Fig. 1 shows a diagram of the manufacturing procedure for the extruded DFRCC panel. The pulverulent material and fiber were mixed by using an omni mixer. Wet-mixing was then performed twice by using a kneader mixer for a period of 3 minutes. Finally, extrusion was performed. The processing time included dry-mixing for 4 minutes, wet-mixing for 6 minutes and extrusion for 5 minutes. Figs. 2 and 3 show photographs of the extrusion equipment and the manufacturing process of the extruded DFRCC panel, respectively.

2.2.3 Mix-proportion

A preliminary experiment was performed to determine the mix proportion with a water to binder ratio of 8~12%, a DFRCC powder to binder ratio of 20~30% and a silica to binder ratio of 30~40%. It has been shown that it is hard to mix materials when 0.5% PVA fiber is inserted. In order to prevent the clumping of fibers and to homogeneously disperse the fiber without increasing the water to binder ratio, an alternative mixing method, which is described in Section 2.2.2, was adopted. Hydroxypropylmethyl-cellulose (HPMC, Atex Co., Korea) was inserted. Table 3 shows the 4 mix proportions (which were determined in the preliminary experiment) that were employed to test the flexural behavior of the extruded DFRCC panel.

(a) Pre-mixing

(b) Wet-mixing

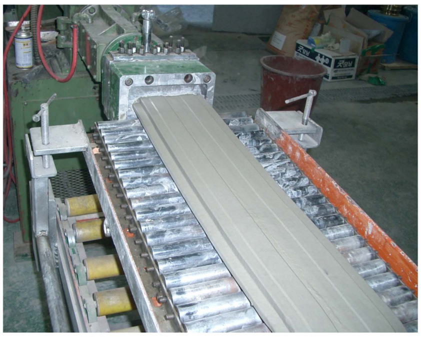

(c) Extruding process of DFRCC panel

Fig. 3 Production of extruded DFRCC panel

Table 3 Mixing properties of extrusion DFRCC panels

Types	Cement	Water	DFRCC powder*	Silica powder	Silica sand	*SP*	HPMC†	PVA (vol.%)
*MX*1	1.0	0.24	0.68	0.93	0.00	0.0053	0.016	2.0
*MX*2	1.0	0.27	0.72	0.77	0.26	0.0056	0.017	2.0
*MX*3	1.0	0.27	0.72	1.0	0.00	0.0056	0.017	2.0
*MX*4	1.0	0.30	0.88	1.1	0.00	0.0061	0.018	2.0

All numbers are mass ratios of cement weight
*DFRCC powder: BFS, Sepiolite, $Mg(OH)_2$, $CaCO_3$, CSA, $Al(OH)_3$, *CW*150
†Hydroxypropylmethyl-cellulose

2.2.4 Curing conditions

Autoclave curing was considered in order to achieve dimensional stability and a fast manufacturing cycle. However, it was impossible to achieve the desired flexural performance due to the melting of fibers at 180~200°C. Therefore, an alternative curing method was considered. To be more specific, the extruded DFRCC panel was pre-cured for 5 hours after extrusion, and then cured at 50°C for a period of 3 days (Fig. 4). Curing the extruded DFRCC for more than 3 days presented challenges due to the manufacturing process. Therefore, it was necessary to test the compressive strength after 3 days. Test results show that at 3 days, the developed compressive strength was more than 30% of

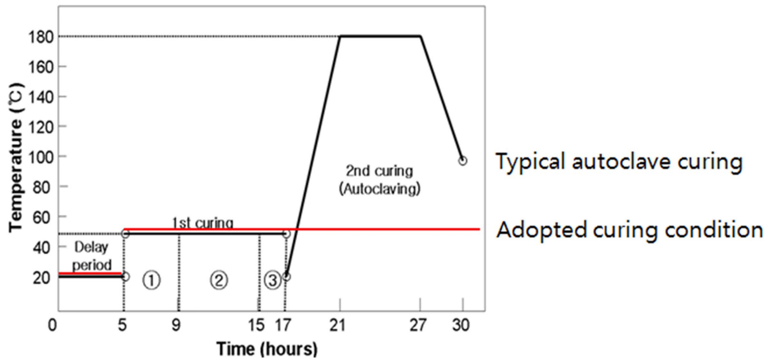

Fig. 4 Curing condition of extruded DFRCC panel

that at 28 days without any deterioration and deformation during storage and curing. Therefore, with the proposed curing method, the manufacturing process can be completed within 3 days without autoclave curing, thus making it a more economical approach.

3. Experiments

3.1 Specimens and experimental method

A four-point bending test was conducted to examine the performance of the extruded DFRCC panel. Fig. 5 shows a specimen whose dimensions are 400 mm × 10 mm × 100 mm. Two specimens

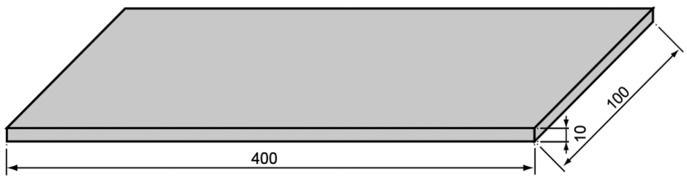

Fig. 5 Specimen geometry

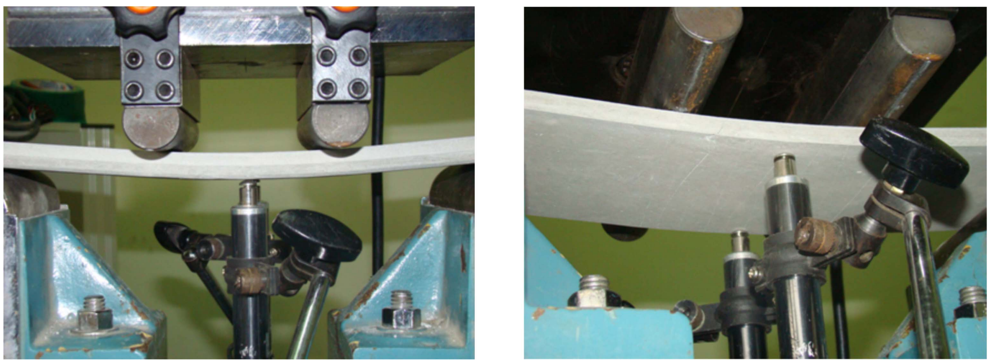

Fig. 6 Flexural test on extruded DFRCC panel

for each experimental variable were manufactured. The tests were carried out through displacement control by using an actuator with a capacity of 250 kN. The deflection at the center of the flexural specimens was measured by means of a Linear Variable Differential Transformer (LVDT) that was installed at the center of each specimen. Fig. 6 illustrates the flexural test apparatus. The flexural strength was calculated by Eq. (5).

$$F_b = \frac{P \times l}{b \times d^2} \tag{5}$$

where F_b is the flexural strength, P is the maximum load, l is the span length, and b and d are the width and height of the specimen, respectively.

3.2 Evaluation technique of fiber distribution

3.2.1 Fiber detection in fiber image

The distribution characteristics of fiber can be quantitatively represented by detecting the fibers in

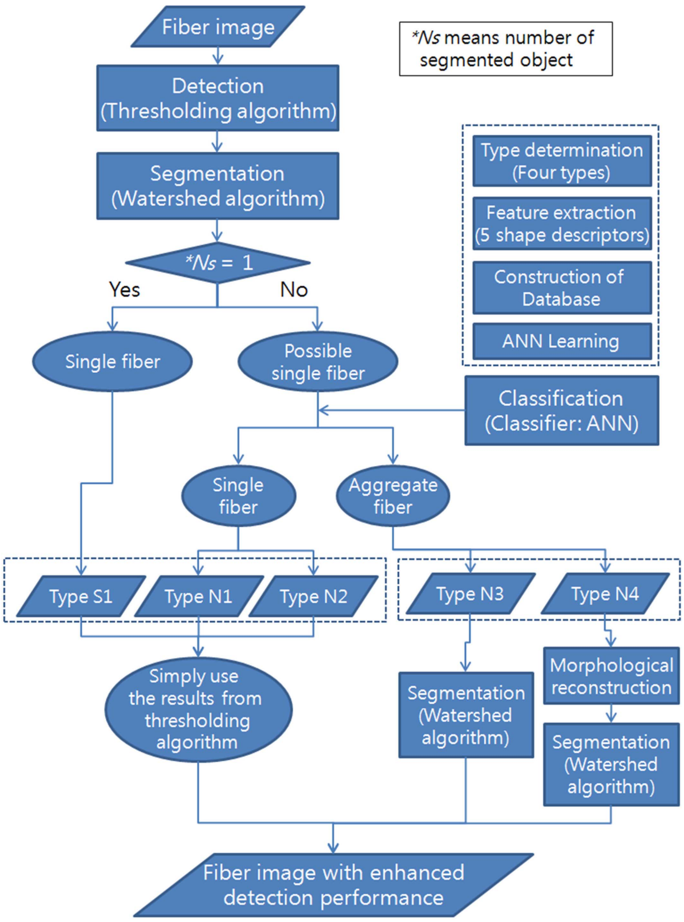

Fig. 7 Flow chart of enhanced detection algorithm (Lee *et al.* 2009)

a fiber image and calculating the distribution coefficient by mathematical treatment. In this study, an enhanced evaluation technique for PVA fiber dispersions in Engineered Cementitious Composites (ECC) was adopted (Lee *et al.* 2009). This technique is essentially composed of tasks. First, the specimen was prepared and treated, followed by acquisition of a fluorescence image by using a fluorescence microscope with a Charged Couple Device (CCD). Based on the proposed image processing algorithm, the fiber images were then automatically detected in a binary image, which was originally converted from the fluorescence image. Next, a mathematical treatment was performed on the data that were obtained from the previous task, which finally provided the calculated fiber dispersion coefficient of the composite.

The image processing technique for detecting fibers is composed of two tasks. First, the fiber images detected by a prototype thresholding algorithm were classified into five types by a watershed segmentation algorithm (Vincent and Soille 1991) and an artificial neural network. Next, aggregate fiber images, (otherwise known as misdetected fiber images) were correctly detected by means of the watershed segmentation algorithm and morphological reconstruction (Vincent 1993). Fig. 7 presents a flow chart of the enhanced detection algorithm.

3.2.2 Fiber distribution coefficient

The degree of fiber dispersion was quantitatively evaluated based on the calculation of the coefficient α_f, which is also referred to as the fiber dispersion coefficient, as expressed by Eq. (6).

$$\alpha_f = \exp\left[-\sqrt{\frac{\sum (x_i - 1)^2}{n}}\right] \tag{6}$$

where n is the total number of fibers on the image and x_i denotes the number of fibers in the i-th unit, which is a square portion that was allocated to the i-th fiber on the assumption that the fiber dispersion was perfectly homogeneous. The value for α_f tends to be 1 for a homogeneous dispersion of fibers, or 0 for a severely biased dispersion.

The second distribution characteristic is the distribution of the fiber orientation. The inclined angle of the fiber to the cutting plane can be calculated by Eq. (7).

$$\theta = \cos^{-1}\left(\frac{l_s}{l_l}\right) \tag{7}$$

where l_s and l_l are the shortest diameter and longest diameter of the fiber image in sectional image, respectively (Fig. 8).

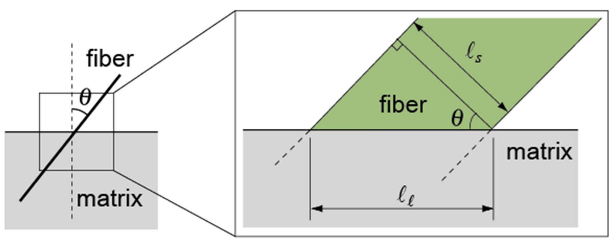

Fig. 8 Schematic diagram of an inclined fiber (Lee *et al.* 2010b)

4. Results and discussion

4.1 Flexural behavior

Table 4 and Fig. 9 present the flexural test results of the extruded DFRCC panel. The *MX*1 specimen exhibits approximately 50 MPa flexural strength, which is the maximum value among the fabricated extruded DFRCC panels, and brittle behavior (low deformation capacity), i.e., a drastic stress drop and low multiple cracking after first cracking due to high matrix strength. On the other hand, the other specimens exhibit deformation hardening behavior after the first cracking. The flexural strength of the *MX*3 and *MX*4 specimens is about 35~38 MPa which is two to four times higher than that of general ECC (10~15 MPa) (Wang *et al.* 2006). The average deflection ratio (δ_b/δ_{bi}), which represents the deformation capacity, and the average number of cracks in the *MX*4 specimens are 9.01 and 11.5, respectively. The *MX*4 specimens exhibit the maximum deformation capacity among the test specimens. The stiffness of the extruded DFRCC panel is measured to be 42.0~53.6 MPa and increases with increasing flexural strength.

4.2 Fiber distribution

Table 5 shows the distribution coefficient that was analyzed according to the specimens by adopting the image processing described in Section 3.2. The fiber images were taken in three random positions with a size of 8×8 mm^2. Fig. 10 shows the fiber images of the *MX*1, *MX*2, *MX*3 and *MX*4 specimens. The fibers in the *MX*4 specimen are more uniformly dispersed in the cross section compared to the others. In particular, the *MX*3, *MX*2 and *MX*1 specimens display the largest fiber dispersion coefficients in the given order, as shown in Table 4 and Fig. 10. Torigoe *et al.* (2003) reported that the deformation capacity of DFRCC increased as the fiber dispersion increased. Therefore, it was predicted that the deformation capacity would decrease in the order of *MX*4, *MX*3, *MX*2 and *MX*1. The flexural test results also exhibited the corresponding results (Fig. 9).

Table 4 Test results of specimens

Specimens	F_{bi} MPa	δ_{bi} mm	F_b MPa	δ_b mm	δ_b/δ_{bi}	Stiffness kN/mm
*MX*1	50.2	0.90	50.2	0.90	1.00	52.2
	36.3	0.69	49.3	1.31	1.90	53.6
*MX*2	30.9	0.67	34.3	2.31	3.45	48.7
	32.0	0.71	38.1	2.18	3.07	46.8
*MX*3	32.6	0.71	37.4	4.95	6.97	46.5
	33.3	0.82	36.7	4.04	4.93	47.1
*MX*4	29.4	0.69	38.6	6.02	8.72	42.2
	28.7	0.66	35.4	6.20	9.39	42.0

F_{bi} : Flexural strength at initial crack
δ_{bi} : Mid-span deflection at F_{bi}
F_b : Maximum flexural strength
δ_b : Mid-span deflection at F_b

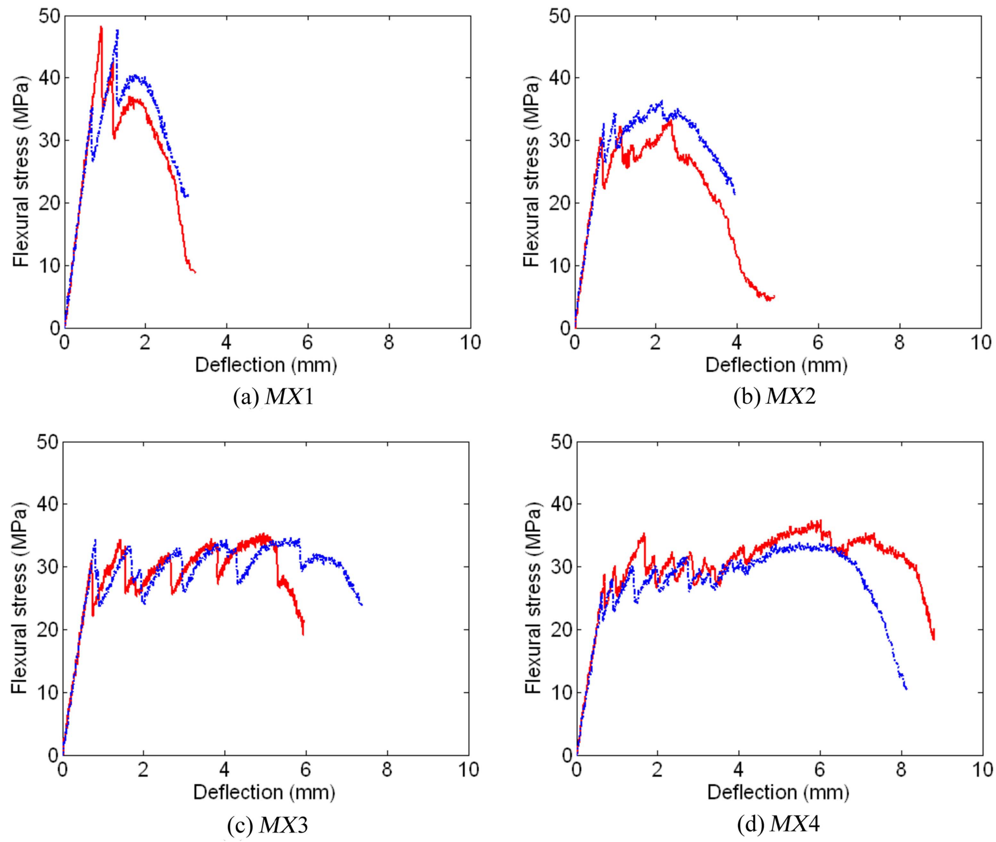

Fig. 9 Flexural stress vs. mid-span deflection curves of DFRCC extrusion panels

Table 5 Test results of specimens

Specimens	α_f	θ (º)
*MX*1	0.27±0.032 0.27±0.050	40±1.8 41±2.7
*MX*2	0.29±0.025 0.27±0.069	43±2.3 39±4.0
*MX*3	0.28±0.055 0.31±0.028	39±2.5 38±1.8
*MX*4	0.33±0.066 0.30±0.016	38±2.9 38±1.1

There was no significant difference in the fiber orientation according to the specimens. The average fiber orientation of the *MX*3 and *MX*4 specimens was about 38°. On the other hand, the average fiber orientation of the *MX*1 and *MX*2 specimens was about 41°. When the fiber orientation was assumed to have a three-dimensional random distribution, then the fiber orientation was 57.3°. When the fiber orientation was assumed to have a two-dimensional random distribution, then the

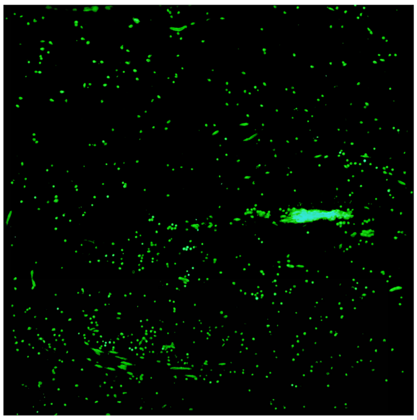

(a) *MX*1

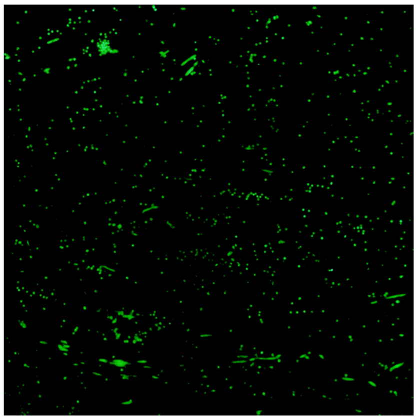

(b) *MX*2

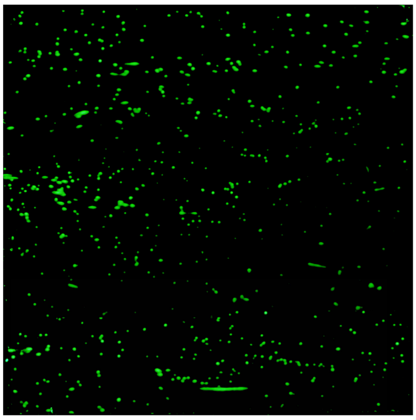

(c) *MX*3

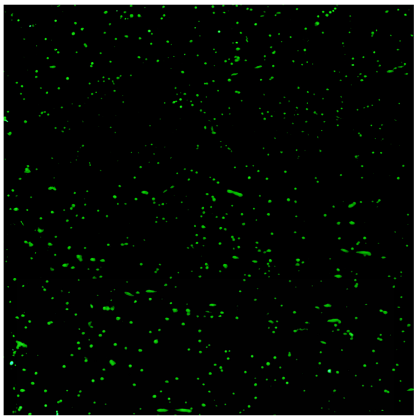

(d) *MX*4

Fig. 10 Typical fiber images

fiber orientation was 45°. Therefore, the fibers of the extruded DFRCC were aligned more than those that were obtained by assuming a two-dimensional random distribution through extrusion process.

Fig. 11 shows the probability density function for the fiber orientation according to the specimens. As can be seen in the figure, the probability density functions measured by the image analysis are considerably different from those obtained when two- or three-dimensional random distributions were assumed for the fiber orientation.

4.3 Correlation between flexural behavior and fiber distribution

The flexural behavior and fiber distribution characteristics of extruded DFRCC vary according to the mix proportion. In this study, it was assumed that the difference in the mix proportion can lead to a difference in fiber distribution, which is the primary factor for the flexural behavior of extruded DFRCC. The test results were analyzed on the basis of this assumption. Fig. 12 shows the fiber bridging curves that were theoretically calculated on the basis of the fiber bridging constitutive law

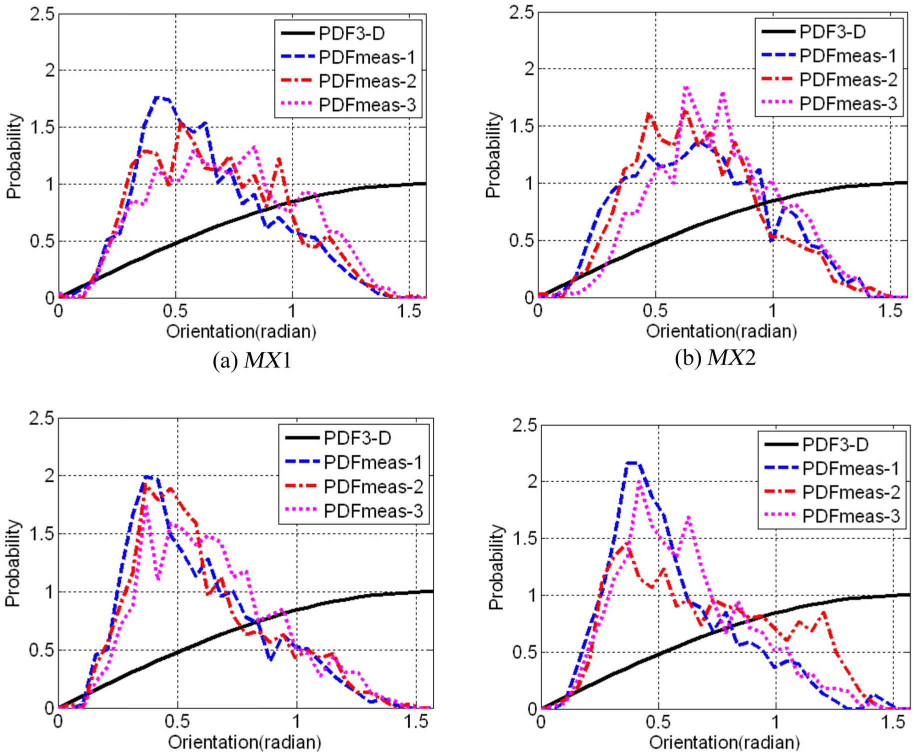

(a) $MX1$ (b) $MX2$

(c) $MX3$ (d) $MX4$

Fig. 11 Typical probability density function of fiber orientation

(Lee *et al.* 2010b) using the experimentally determined probability density function for the fiber orientation that is shown in Fig. 11 and micro-mechanical parameters. The micro-mechanical parameters that were related to the fibers are listed in Table 2. The frictional bond strength was assumed to be 2.9 MPa on the basis of experimental results reported by Kim *et al.* (2007). The chemical bond strength was also assumed to be 1.85 J/m^2 on the basis of experimental results obtained by Li *et al.* (2002).

As described in Section 2.1, the behavior of DFRCC was governed by the fracture toughness of the matrix (J_{tip}), the strength of the matrix (f_t), and the fiber bridging characteristics. The potential of pseudo deformation hardening behavior increases when the fracture toughness and matrix strength decreased and the peak bridging stress increased. J_{tip} of the $MX1$ specimens was higher than the other specimens because the water to binder ratio of these specimens was lower than that of the other specimens. In particular, J_{tip} of the $MX1$ specimens was 94.3% higher than that of the $MX4$ specimens when J_{tip} was calculated indirectly on the basis of F_{bi}, which led to a lower potential for pseudo deformation-hardening behavior (Kim *et al.* 2007). The fiber dispersion coefficient of the $MX1$ specimens was about 14% lower than that of the $MX4$ specimens. As shown in Fig. 12 and Table 6, the $MX1$ specimens exhibit the lowest $J_b^{'}$ and σ_0, which are 40.9% and 9.98% lower than those of the $MX4$ specimens, respectively, which lead to the lowest flexural tension capacity. J_{tip} of the $MX2$ specimens, which incorporated silica sand with a large diameter, was 14.1% higher than that of the $MX4$ specimens when J_{tip} was calculated indirectly on the basis of F_{bi}, which led to a

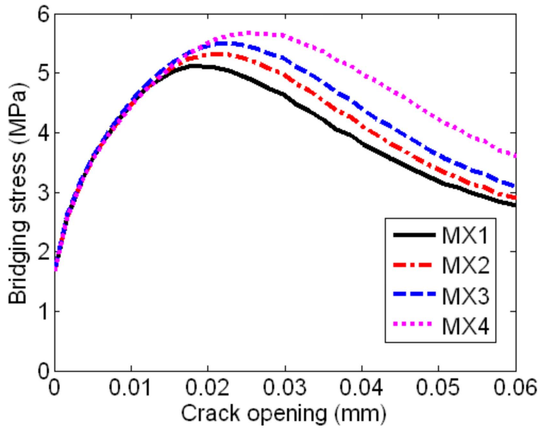

Fig. 12 Comparison of representative fiber bridging curves according to mix-proportions

Table 6 Micro-mechanical analysis

	*MX*1	*MX*2	*MX*3	*MX*4
σ_0	5.11	5.33	5.44	5.67
J_b'	70.6	89.5	99.3	119
J_b'/J_{tip} *	7.06	8.95	9.93	11.9

*J_{tip} is assumed to be 10 J/m^2

lower potential for pseudo deformation-hardening behavior. The fiber dispersion coefficient of the *MX*2 specimens was about 11.0% lower than that of the *MX*4 specimens. Due to these two phenomena, the flexural tension capacity of the *MX*2 specimens was lower than that of the *MX*3 and *MX*4 specimens.

Table 6 shows the toughness ratio (J'_b/J_{tip}) according to the four mix proportions. In Table 6, J_{tip} is assumed to be 10 J/m^2, which is calculated on the basis of a previous research (Lee 2009). It was assumed that the fracture toughness of the matrix was linearly related to the strength of the matrix, because the matrix used in DFRCC showed a linear elastic behavior compared to the concrete. Therefore, the fracture toughness at the crack tip of the extruded DFRCC was increased about nine-fold relative to that of the general ECC, because the flexural strength of extruded DFRCC was three times greater than that of the general ECC. Based on the assumption that J_{tip} was assumed to be 10 J/m^2, the energy criterion was satisfied (Table 6).

The potential for pseudo deformation-hardening behavior of the *MX*3 and *MX*4 specimens was greater than that of the *MX*1 and *MX*2 specimens, which was attributed to the good fiber dispersion and high J_b' and σ_0 of the *MX*3 and *MX*4 specimens. The deformation capacity of the *MX*4 specimens was higher than that of the *MX*3 specimens. This could more readily be explained on the basis of the fiber dispersion of the *MX*4 specimens being about 6.3% higher than that of the *MX*3 specimens and optimal micromechanical parameters for higher deformation capacity.

5. Conclusions

This paper presents a theoretical and experimental study on the manufacture of an extruded DFRCC panel, which exhibited multiple cracking and high deformation capacity, and the effect of fiber distribution characteristics on the flexural behavior of the panel. The following conclusions can be drawn from the current results:

(1) The extruded DFRCC, which exhibited deformation hardening behavior, can be made with dry mixing of materials and 2% PVA fiber, wet-mixing, extrusion and high temperature curing. The extruded DFRCC panel exhibited a maximum deformation capacity when the ratios of water, DFRCC powder and silica powder to cement were 0.30, 0.88 and 1.1, respectively. The stiffness of the extruded DFRCC panel increased when the flexural strength increased.

(2) The fiber dispersion was found to be better when the flexural deformation capacity increased. The average fiber orientation of the specimens was about 39.5°. If the fiber orientation was assumed to have two- and three-dimensional random distributions, then the fiber orientation was 45.0° and 57.3°, respectively. In terms of the average fiber orientation, it was found that fibers are aligned to the direction of extrusion than fiber orientation given with the assumption of a two-dimensional random distribution. The probability density functions measured by the image analysis were considerably different from those obtained when two- or three-dimensional random distributions were assumed for the fiber orientation.

(3) The mechanical properties are influenced by micromechanical parameters such as matrix, fiber and interfacial properties as well as fiber orientation and dispersion. The fiber distribution varied according to the mix proportion with the same extrusion process, which led to differences in the flexural behavior. Therefore, it is necessary to consider micromechanical parameters and the fiber distribution characteristics, as well as the manufacturing process, in order to achieve a desired performance, such as flexural strength and deformation capacity.

Ackwnowledgements

This research was supported by a grant (11CHUD-C058202-01) from High tech Urban Development Program funded by Ministry of Land, Transportation and Maritime Affairs of Korean government and also supported by the grant of the Korean Ministry of Education, Science and Technology (The Regional Core Research Program/Biohousing Research Institute) and the Biohousing Research Center.

References

Akkaya, Y., Peled, A. and Shah, S.P. (2000), “Parameters related to fiber length and processing in cementitious composites”, *Mater. Struct.*, **33**(8), 525-524.

Fu, S.Y. and Lauke, B. (1996), “Effects of fiber length and fiber orientation distributions on the tensile strength of short-fiber-reinforced polymers”, *Compos. Sci. Technol.*, **56**(10), 1179-1190.

Kanda, T. and Li, V.C. (2006), “Practical design criteria for saturated pseudo strain hardening behavior in ECC”, *J. Adv. Concrete Technol.*, **4**(1), 59-72.

Kim, J.K., Kim, J.S., Ha, G.J. and Kim, Y.Y. (2007), “tensile and fiber dispersion performance of ECC produced with ground granulated blast furnace slag”, *Cement Concrete Res.*, **37**(7), 1096-1105.

Lee, B.Y. (2009), "Fiber distribution evaluation using digital image processing and its effect on tensile behavior of fiber reinforced cement composites", PhD Thesis, KAIST.

Lee, B.Y., Kim, J.K., Kim, J.S. and Kim, Y.Y. (2009), "Quantitative evaluation technique of pva (polyvinyl alcohol) fiber dispersion in engineered cementitious composites", *Cement Concrete Comp.,* **31**(6), 408-417.

Lee, B.Y., Kim, J.K. and Kim, Y.Y. (2010a), "Prediction of ECC tensile stress-strain curves based on modified fiber bridging relations considering fiber distribution characteristics", *Comput. Concrete*, **7**(5), 455-468.

Lee, B.Y., Lee, Y., Kim, J.K. and Kim, Y.Y. (2010b), "Micromechanics-based fiber-bridging analysis of strain-hardening cementitious composite accounting for fiber distribution", *CMES-Comp. Model. Eng.,* **61**(2), 111-132.

Leung, C.K.Y. (1996), "Design criteria for pseudoductile fiber-reinforced composites", *J. Eng. Mech.-ASCE,* **122**(1), 10-14.

Li, V.C. and Leung, K.Y. (1992), "Steady-state and multiple cracking of short random fiber composites", *J. Eng. Mech.-ASCE,* **118**(11), 2246-2264.

Li, V.C., Wu, C., Wang, S., Ogawa, A. and Saito, T. (2002), "Interface tailoring for strain-hardening PVA-ECC", *ACI Mater. J.,* **99**(5), 463-472.

Marshall, D.B. and Cox, B.N. (1988), "A J-integral method for calculating steady-state matrix cracking stressed in composites", *Mech. Mater.,* **7**(2), 127-133.

Roth, M.J., Slawson, T.R. and Flores, O.G. (2010), "Flexural and tensile properties of a glass fiber-reinforced ultra-high-strength concrete: an experimental, micromechanical and numerical study", *Comput. Concrete,* **7**(2), 169-190.

Shao, Y. and Shah, S.P. (1997), "Mechanical properties of PVA fiber reinforced cement composites fabricated by extrusion processing", *ACI Mater. J.,* **94**(6), 555-564.

Shao, Y., Markunte, S. and Shah, S.P. (1995), "Extruded fiber-reinforced composites", *Concrete Int.*, **17**(4), 48-53.

Stang, H. and Li, V.C. (1999), "Extrusion of ECC-Material", *Proceedings of High Performance Fiber Reinforced Cement Composites 3* (Reinhardt and Naaman, A. (eds)), Chapman & Hull, 203-212.

Takashima, H., Miyagai, K., Hashida, T. and Li, V.C. (2003), "A design approach for the mechanical properties of polypropylene discontinuous fiber reinforced cementitious composites by extrusion molding", *Eng. Fract. Mech.,* **70**(7), 853-870.

Torigoe, S., Horikoshi, T. and Ogawa, A. (2003), "Study on evaluation method for PVA fiber distribution in engineered cementitious composite", *J. Adv. Concrete Technol.,* **1**(3), 265-268.

Vincent, L. (1993), "Morphological grayscale reconstruction in image analysis: applications and efficient algorithms", *IEEE T. Image Process.,* **2**(2), 176-201.

Vincent, L. and Soille, P. (1991), "Watesheds in digital spaces: An efficient algorithm based on immersion simulations",. *IEEE T. Pattern Anal.,* **13**(6), 583-598.

Wang, S. and Li, V.C. (2006), "Polyvinyl alcohol fiber reinforced engineered cementitious composites: material design and performances", *Proceedings of Int'l RILEM Workshop on HPFRCC in Structural Applications*, RILEM SARL, 65-73.

CC